Electron-phonon interactions for optical-phonon modes in few-layer graphene: First-principles calculations

Jia-An Yan, W. Y. Ruan, and M. Y. Chou
School of Physics, Georgia Institute of Technology, Atlanta, Georgia 30332 USA
(Received 3 December 2008; revised manuscript received 17 February 2009; published 30 March 2009)

We present a first-principles study of the electron-phonon (*e*-ph) interactions and their contributions to the linewidths for the optical-phonon modes at Γ and *K* in one-layer to three-layer graphene. It is found that, due to the interlayer coupling and the stacking geometry, the high-frequency optical-phonon modes in few-layer graphene couple with different valence and conduction bands, giving rise to different *e*-ph interaction strengths for these modes. Some of the multilayer optical modes derived from the Γ-E_{2g} mode of monolayer graphene exhibit slightly higher frequencies and much reduced linewidths. In addition, the linewidths of *K*-A_1' related modes in multilayers depend on the stacking pattern and decrease with increasing layer numbers.

DOI: 10.1103/PhysRevB.79.115443 PACS number(s): 63.22.−m, 63.20.kd, 73.21.Ac, 71.38.−k

I. INTRODUCTION

The possibilities of developing carbon-based nanostructures for electronics applications have stimulated recent interest in graphene and its derivatives.[1–3] One of the focus areas is to understand the scattering processes of electrons. In carbon nanotubes and graphite, the high currents or optical excitations have been shown to induce a significant overpopulation of the optical-phonon modes of E_{2g} at Γ (Γ-E_{2g}) and A_1' at *K* (*K*-A_1').[4–6] Since these phonon modes exhibit strong electron-phonon (*e*-ph) interactions, overpopulation of them leads to a dramatic reduction in the ballistic conductance of carbon nanotubes at high bias potentials,[4] and consequently interconnect performance deteriorates.[7] Understanding the phonon decays[8] from a microscopic point of view, in particular, based on the *e*-ph interaction, is thus a key step to improve the transport properties of these materials and to control device performance. Furthermore, the *e*-ph interaction also plays a significant role in many phenomena such as the quasiparticle dynamics and anomalies in photoemission spectra,[9–13] Raman scattering,[14] and superconductivity.[15]

Experimentally, the linewidths of the zone-center phonon modes obtained from Raman or infrared (IR) measurements contain significant contributions from the *e*-ph interaction.[16] In graphene, the phonon linewidth of the Γ-E_{2g} mode is estimated to be about 13 cm^{-1} based on the Raman spectra.[17] In graphite, the graphene E_{2g} mode splits into two branches: the Raman-active E_{2g} and IR-active E_{1u} modes. The linewidth of the Raman-active mode (11.5 cm^{-1}) is almost the same as that of graphene[18] while IR measurements show that the linewidth of the E_{1u} mode is surprisingly much smaller.[19]

Few-layer graphene (FLG) presents an interesting system because of the possibility to tune its electronic properties.[20] In the epitaxially grown graphene, FLG is often produced as a main product.[1] Depending on the layer number and stacking geometry,[21] the linear band dispersions in monolayer graphene evolve into several bands due to the interlayer coupling in FLG.[21,22] Similarly, the E_{2g} mode at Γ and A_1' mode at *K* in single layer also split into several branches.[23] It is expected that the *e*-ph interaction will be significantly modified as the number of layers and stacking geometry are varied.

In this work, we performed first-principles calculations of the *e*-ph interactions in one-layer, two-layer (AB stacking), and three-layer (ABA and ABC stackings) graphenes. The Γ-E_{2g} and *K*-A_1' modes in graphene, which are, respectively, coupled to intravalley and intervalley electronic scatterings, have much stronger *e*-ph interactions than other modes.[24] Here we focus on these two modes and their derivatives in FLGs in order to investigate the stacking effect. We found that, while the weak interlayer interaction gives rise to only small splittings of these phonon modes, the resulting *e*-ph interactions for some of them are considerably suppressed because of symmetry constraints.

II. CALCULATION DETAILS

The *e*-ph matrix element $g^{\nu}_{(\mathbf{k}+\mathbf{q})j',\mathbf{k}j}$ is defined as

$$g^{\nu}_{(\mathbf{k}+\mathbf{q})j',\mathbf{k}j} = \sqrt{\frac{\hbar}{2M\omega^{\nu}_{\mathbf{q}}}}\langle \mathbf{k}+\mathbf{q},j'|\frac{\delta V_{\mathrm{scf}}}{\delta u^{\nu}_{\mathbf{q}}}|\mathbf{k},j\rangle, \qquad (1)$$

where $\delta V_{\mathrm{scf}} \equiv V_{\mathrm{scf}}(u^{\nu}_{\mathbf{q}}) - V_{\mathrm{scf}}(0)$ is the variation in the self-consistent potential field due to the perturbation of a phonon with wave vector $\mathbf{q}$ and branch index ν. $|\mathbf{k},j\rangle$ is the electronic Bloch state. We further define the *e*-ph coupling strength between phonon mode $\mathbf{q}\nu$, and Bloch states $|\mathbf{k}+\mathbf{q},j'\rangle$ and $|\mathbf{k},j\rangle$ as $g^2_{j'j}(\mathbf{k}) = |g^{\nu}_{(\mathbf{k}+\mathbf{q})j',\mathbf{k}j}|^2$.

The electronic states and the self-consistent field were computed using the first-principles codes QUANTUM ESPRESSO (Refs. 25 and 26) and the perturbation of a phonon mode was handled with the frozen-phonon approach. Figure 1(a) shows the supercell used in the frozen-phonon calculation for the *K* phonons. The electronic structure was calculated with the local-density approximation (LDA) within density-functional theory, and the core-valence interaction was modeled by norm-conserving pseudopotentials.[27] Wave functions of the valence electrons were expanded in plane waves with a kinetic-energy cutoff of 70 Ry. The phonon frequencies and associated eigenvectors were computed using the density-functional perturbation theory (DFPT),[25] details of which have been presented in our previous work.[23] A vacuum region of 10 Å was introduced in our supercell to eliminate the artificial interaction between neighboring su-

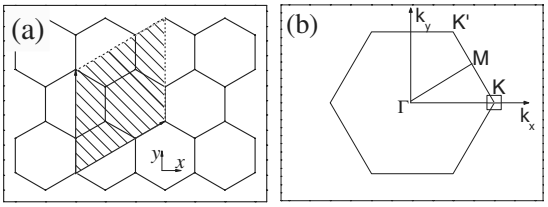

FIG. 1. (a) Supercell (shaded area) used in the frozen-phonon calculation for the K phonon modes in few-layer graphene. (b) First Brillouin zone of the primitive unit cell of graphene. The square area for the dense $\mathbf{k}$-grid sampling is indicated.

percells along the z direction. The relaxed C-C bond length is 1.42 Å and the interlayer distance is 3.32 Å for all FLGs considered in this paper. Variations in the potential fields δV_{scf} were calculated through self-consistent calculations to find the potential field for both perturbed and unperturbed systems. The following calculations were carried out on a dense 100×100 k grid within a small square area enclosing point K in reciprocal space, as indicated in Fig. 1(b), in order to obtain the electronic wave functions at $\mathbf{k}$ and $\mathbf{k}+\mathbf{q}$ near the Fermi level. This dense k sampling was found necessary for a quantitative description of the scattering process near the Fermi level in one-layer and few-layer graphenes. Finally, the e-ph interaction matrix elements were computed using Eq. (1).

In order to check the accuracy of our calculations, we first calculate the e-ph matrix elements over the Fermi surface and compare them with previously published results for monolayer graphene. Due to the electronic degeneracy at K, the averaged e-ph matrix elements for all possible pairs are $\langle g^2_{\Gamma}\rangle_F=\Sigma_{i,j}|g_{(\mathbf{K})i,\mathbf{K}j}|^2/4=0.0401$ eV^2 for the Γ-E_{2g} mode, and $\langle g^2_{\mathbf{K}}\rangle_F=\Sigma_{i,j}|g_{(2\mathbf{K})i,\mathbf{K}j}|^2/4=0.0986$ eV^2 for the K-A_1' mode, respectively. These results are in excellent agreement with those in previous DFPT calculations (0.0405 and 0.0994 eV^2, respectively).[28]

The phonon linewidth γ due to the e-ph coupling is defined as[29]

$$\gamma^{\mathbf{q}\nu}=\frac{4\pi}{N_k}\sum_{\mathbf{k}jj'}|g^{\nu}_{(\mathbf{k}+\mathbf{q})j',\mathbf{k}j}|^2[f_{\mathbf{k}j}-f_{(\mathbf{k}+\mathbf{q})j'}]\times\delta[\varepsilon_{\mathbf{k}j}-\varepsilon_{(\mathbf{k}+\mathbf{q})j'}+\hbar\omega^{\nu}_{\mathbf{q}}], \quad (2)$$

with $f_{\mathbf{k}j}$ being the Fermi-Dirac occupation function for Bloch state $|\mathbf{k},j\rangle$. An energy smearing parameter is needed in order to handle the δ function in Eq. (2). With our k-point grid, we have found that the result varies little after the smearing parameter is increased to 0.01 eV. As for the temperature dependence, we find that the result for the Γ-E_{2g} mode in graphene calculated from Eq. (2) shows weak dependence on the temperature below $k_BT=20$ meV. Above that the linewidth decreases as temperature increases, resulting from the electronic occupation change near the Fermi level.[7] For all the linewidths calculated below, we used a broadening parameter of 0.01 eV for the δ function in Eq. (2), and $k_BT=2.5$ meV for the Fermi-Dirac distribution.

III. RESULTS AND DISCUSSIONS

Table I lists the calculated phonon linewidths due to the e-ph coupling. For the monolayer, the linewidth γ of the degenerate Γ-E_{2g} modes is 11.2 cm^{-1}, in reasonable agreement with experimental observation[17] of 15.0 cm^{-1} and previously published result[18] of 11.5 cm^{-1}. A value of 20.4 cm^{-1} is obtained for the highest optical K-A_1' mode. In FLGs, the phonon modes split into branches with different symmetries. Consequently, their linewidths can be quite different from one another. In the AB bilayer, for example, the original highest Γ phonon splits into the Raman-active E_g and IR-active E_u modes. While the linewidth of the E_g mode (8.6 cm^{-1}) is only slightly smaller than that of the monolayer (11.2 cm^{-1}), the linewidth of the E_u mode is two orders of magnitude smaller. The calculated linewidth of the E_g mode is consistent with recent experimental observation of 13.5 cm^{-1} for the Γ optical-phonon mode in bilayer graphene.[30] Similar results for the monolayer and bilayer graphenes were also reported by Park *et al.*[31] For the ABA and ABC trilayers, the results in Table I show different behavior for different modes. In particular, for the ABC trilayer two out of three optical modes at Γ show reduced electron-phonon interaction. Most importantly, the linewidths of all K phonons in Table I drop significantly as the layer number increases from one to three. This indicates that the interlayer interaction can effectively suppress valley-spin decoherence via e-ph scatterings, making the FLGs more attractive as valleytronic materials.[32,33]

As a comparison, we also calculated the linewidths for the high-frequency modes in bulk graphite with an infinite AB stacking. The linewidths for the averaged E_{2g} and E_{1u} modes

TABLE I. Calculated phonon linewidth γ (in cm^{-1}) for the high-frequency optical-phonon modes at Γ and K in monolayer, bilayer, and trilayer graphenes. The mode symmetries S and the frequencies ω (in cm^{-1}) are also listed for completeness.

	Monolayer			AB			ABA			ABC		
	S	ω	γ	S	ω	γ	S	ω	γ	S	ω	γ
Γ	E_{2g}	1586	11.2	E_g	1587	8.6	E_a'	1586	9.7	$E_{g,a}$	1586	7.2
				E_u	1592	0.1	E''	1588	11.0	E_u	1589	0.0
							E_b'	1593	2.8	$E_{g,b}$	1594	0.3
K	A_1'	1306	20.4	E	1318	9.0	E_1', E_1''	1316	8.4	E	1318	2.8
							E_2'	1324	3.6	A_1	1325	2.2

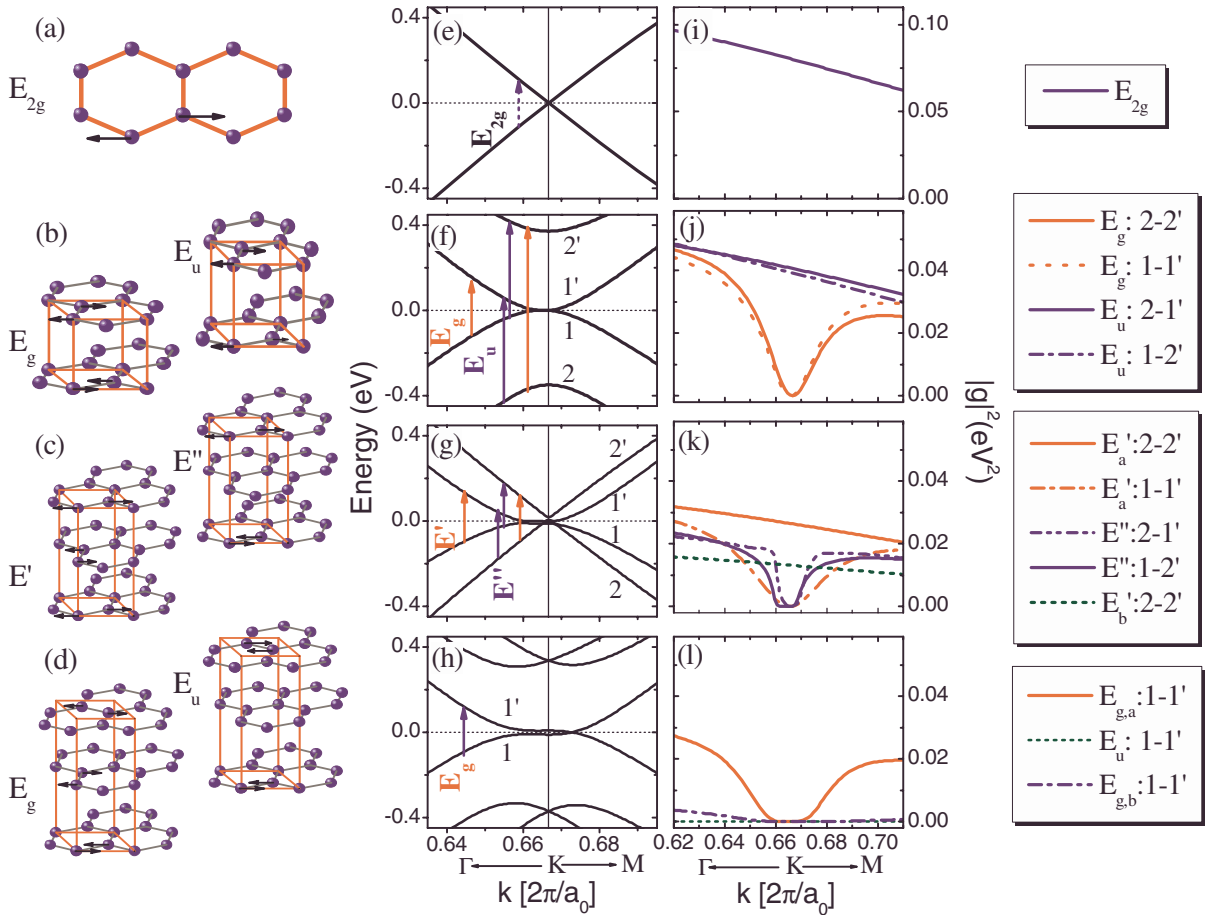

FIG. 2. (Color online) [(a)–(d)] Optical modes at Γ, [(e)–(h)] band dispersions near the Fermi level, and [(i)–(l)] the square of the *e*-ph interaction strength $|g|^2$ of the optical modes at Γ for monolayer, AB bilayer, ABA, and ABC trilayer graphenes, respectively. Symmetry-allowed transitions from valence bands to conduction bands with nonzero strength are shown. The red (light) and blue (dark) lines in (e)–(l) denote transitions for the different modes.

at the zone center are calculated to be 9.7 and 2.2 cm^{-1}, respectively, which are in good agreement with previous theoretical work.[7] For the *E* mode at *K*, the linewidth is found to be 9.8 cm^{-1}. These results are close to those of AB bilayer graphene.

For FLGs there are a few valence and conduction π bands near the Fermi energy level. The symmetry-allowed interband transitions by the absorption of a phonon are indicated in the middle column of Fig. 2. To examine the contributions of different electronic states to the *e*-ph coupling strengths in FLGs, we present in the right column of Fig. 2 the absolute value squared of the *e*-ph coupling matrix elements for optical phonons at Γ as a function of electronic crystal momentum $\mathbf{k}$ along the symmetry line Γ-*K* for all symmetry-allowed transitions. Some of these matrix elements decrease monotonically with increasing k_x, as in the case of monolayer; some of them show a minimum at *K*. These features are closely related to the symmetry of the electronic states near *K* in the presence of interlayer interactions, and can be further quantitatively understood using a tight-binding model. Following the procedures in Refs. 34 and 35, we obtain the *e*-ph matrix element for the in-plane optical-phonon mode $\mathbf{q}\nu$ in *L*-layer graphene as

$$g^{\nu}_{(\mathbf{k}+\mathbf{q})j',\mathbf{k}j} = g_0 \sum_{l=1}^{L} \{[\vec{t}(\mathbf{k}) \cdot \vec{\epsilon}^{\nu}_{l\alpha}(\mathbf{q}) - \vec{t}(\mathbf{k}+\mathbf{q}) \cdot \vec{\epsilon}^{\nu}_{l\beta}(\mathbf{q})] \times u^{*}_{l\alpha,j'}(\mathbf{k}+\mathbf{q}) u_{l\beta,j}(\mathbf{k}) + [\vec{t}(-\mathbf{k}-\mathbf{q}) \cdot \vec{\epsilon}^{\nu}_{l\alpha}(\mathbf{q}) - \vec{t}(-\mathbf{k}) \cdot \vec{\epsilon}^{\nu}_{l\beta}(\mathbf{q})] \times u^{*}_{l\beta,j'}(\mathbf{k}+\mathbf{q}) u_{l\alpha,j}(\mathbf{k})\} \quad (3)$$

$$\equiv g_0 U^{\dagger}_{j'}(\mathbf{k}+\mathbf{q}) \Phi^{\nu}(\mathbf{k},\mathbf{q}) U_j(\mathbf{k}), \quad (4)$$

with $U^{\dagger}_j(\mathbf{k}) = [u^{*}_{1\alpha,j}(\mathbf{k}), u^{*}_{1\beta,j}(\mathbf{k}), u^{*}_{2\alpha,j}(\mathbf{k}), u^{*}_{2\beta,j}(\mathbf{k}), \ldots]$ being the tight-binding amplitudes of band *j* for each site in the unit cell. $\vec{\epsilon}_{l\alpha}$ and $\vec{\epsilon}_{l\beta}$ are the vibrational eigenvectors for the two atoms in layer *l*. $\vec{t}(\mathbf{k}) = \Sigma_{i=1}^{3} \hat{\delta}_i e^{i\mathbf{k}\cdot\mathbf{R}_i}$, where $\hat{\delta}_i$'s $(i=1-3)$ are the unit vectors connecting atom α in layer *l* to its three nearest neighbors (NNs), and $\mathbf{R}_i$ are the lattice vectors of the unit cells in which the three NNs are located. The constant $g_0 = J\Omega^{1/2}/(\omega^{\nu}_{\mathbf{q}}\sqrt{M})$ depends on the mode frequency $\omega^{\nu}_{\mathbf{q}}$, the

e-ph interaction parameter J, the area of the unit cell Ω, and the carbon atomic mass M. The coupling matrix $\Phi^{\nu}(\mathbf{k},\mathbf{q})$ has the form:

$$\Phi^{\nu}(\mathbf{k},\mathbf{q}) = \begin{pmatrix} \Phi_1 & & & \\ & \Phi_2 & & \\ & & \ddots & \\ & & & \Phi_L \end{pmatrix}, \tag{5}$$

with

$$\Phi_l = \begin{pmatrix} 0 & \vec{t}(\mathbf{k}) \cdot \vec{\epsilon}^{\nu}_{l\alpha}(\mathbf{q}) - \vec{t}(\mathbf{k}+\mathbf{q}) \cdot \vec{\epsilon}^{\nu}_{l\beta}(\mathbf{q}) \\ \vec{t}^{\,*}(\mathbf{k}+\mathbf{q}) \cdot \vec{\epsilon}^{\nu}_{l\alpha}(\mathbf{q}) - \vec{t}^{\,*}(\mathbf{k}) \cdot \vec{\epsilon}^{\nu}_{l\beta}(\mathbf{q}) & 0 \end{pmatrix}. \tag{6}$$

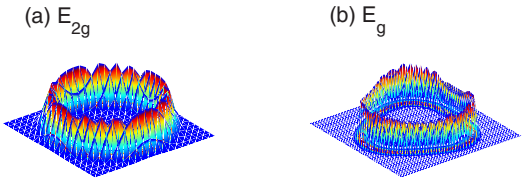

FIG. 4. (Color online) Electronic momentum-resolved contributions of all scattering processes to the phonon linewidth for the doubly degenerate (a) E_{2g} mode in monolayer graphene and (b) E_g mode in bilayer graphene. Note that only $-0.009 \leq k_x, k_y \leq 0.009$ for monolayer and $-0.021 \leq k_x, k_y \leq 0.021$ for bilayer are shown. k_x and k_y are in $2\pi/a_0$.

It is clear that the e-ph interaction strength depends on the orbital characteristics of the initial and final electronic states as well as the displacement pattern of the phonon mode. Note that Φ_l is an off-diagonal matrix, coupling the electronic component of one sublattice to that of the other sublattice in each layer through phonon displacements in the same layer. The coupling effects in different layers will be summed up in either a constructive or a destructive way, depending on the relative phase of the phonon displacements in different layers and the relative phase of the tight-binding amplitudes in the initial and final electronic states involved.

As an example, Fig. 3 schematically shows the symmetry-allowed transitions through the E_g and E_u modes at Γ between valence and conduction bands in bilayer graphene. The four relevant energy bands shown in Fig. 2(f) are indexed as 2, 1, $1'$, and $2'$ from lower valence bands to higher conduction bands. For the E_g mode, the in-plane vibrations of α and β atoms in neighboring planes are in phase. Taking into account the symmetry of electronic wave function in each layer, allowed transitions turn out to be $1 \rightarrow 1'$ and $2 \rightarrow 2'$. As $\mathbf{k}$ approaches K, the four bands become parabolic and the wave-function amplitudes tend to be localized on one sublattice of each layer. Since the transition matrix elements for $1 \rightarrow 1'$ and $2 \rightarrow 2'$ contain product of the electronic wave functions on both sublattices, small wave-function amplitudes give rise to vanishingly small matrix elements near K, as shown in Fig. 2(j). On the other hand, the E_u mode involves in-plane vibrations of α and β atoms in neighboring planes that are out of phase. The symmetry-allowed transitions are $2 \rightarrow 1'$ and $1 \rightarrow 2'$. Even though the wave-function amplitude at one sublattice may become small when $\mathbf{k}$ approaches K, the products with wave-function amplitudes at the other sublattice are still finite. Therefore, the matrix elements exhibit similar linear behavior as in monolayer graphene.

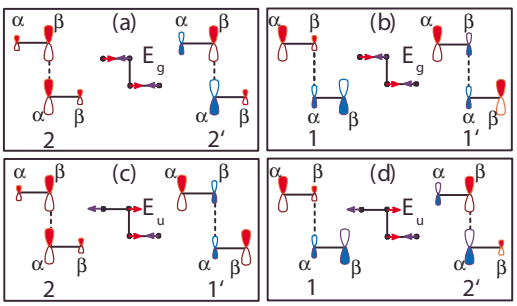

FIG. 3. (Color online) Schematic diagrams of electronic orbitals and optical-phonon modes at Γ that give rise to nonzero e-ph matrix elements in bilayer graphene. The tight-binding orbitals of each band close to K are shown. The filled part indicates the positive portion of the π orbital.

In collecting the contributions from different $\mathbf{k}$ states to calculate the phonon linewidth in Eq. (2), energy conservation is controlled by the delta function. For the E_g mode, this condition can be satisfied in the transition $1 \rightarrow 1'$ but not in the transition $2 \rightarrow 2'$. Nevertheless, the phonon linewidth listed in Table I is about 3/4 of the value for monolayer graphene. Figure 4 presents the $\mathbf{k}$-resolved linewidth contributions for the doubly degenerate E_{2g} mode in monolayer graphene and the E_g mode in bilayer graphene. Clearly, the contributions are almost isotropic in $\mathbf{k}$ space for the E_{2g} mode in monolayer graphene. The shell shape is a result of energy conservation for the scattering events. Due to the trigonal symmetry of the constant-energy surface in bilayer graphene, the $\mathbf{k}$-dependent contributions show a threefold symmetry for the E_g mode. In contrast, the symmetry-allowed transitions of $2 \rightarrow 1'$ and $1 \rightarrow 2'$ for the E_u mode cannot satisfy the required energy conservation because the energy separation of the initial and final states is too large. This leads to a vanishingly small probability for the E_u mode to decay through the e-ph interaction. These results are a reminiscence of the properties of Γ-E_{2g} and Γ-E_{1u} phonons in bulk graphite regarding their e-ph interactions.[7]

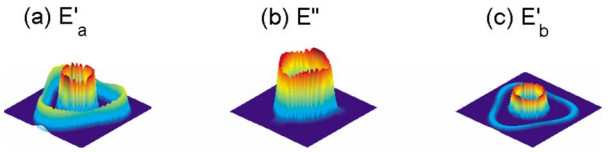

FIG. 5. (Color online) Electronic momentum-resolved contributions of all scattering processes to the phonon linewidth for the (a) E'_a, (b) E'', and (c) E'_b phonon modes at Γ in ABA trilayer graphene. The **k** area shown in the figure is indicated in Fig. 1(b). The origin corresponds to K.

For the ABA trilayer, the four energy bands crossing or touching the Fermi energy are again indexed as 2, 1, 1′, and 2′ in Fig. 2. When a Γ-E'_a phonon is absorbed, both symmetry and energy allowed transitions are $2 \rightarrow 2'$ and $1 \rightarrow 1'$, which manifest themselves as the inner and outer rings, respectively, in Fig. 5(a). When a Γ-E'' phonon is absorbed, the symmetry and energy allowed transitions are $2 \rightarrow 1'$ and $1 \rightarrow 2'$. Incidentally, the energy differences between bands 2 and 1′, and between bands 1 and 2′ are equal for any **k**. Therefore, the rings associated with these two different transitions overlap in Fig. 5(b). The electronic states involved span an energy range of $\hbar\omega \sim 0.2$ eV about the Fermi level. A Γ-E'_b phonon obeys the same selection rule as a Γ-E'_a phonon since both bear the same group representation. The e-ph coupling strength of the former is, however, much weaker than that of the latter.

For the ABC trilayer, the relevant energy bands are indexed as 1 and 1′ in Fig. 2. The three Γ phonons derived from the E_{2g} mode in monolayer graphene are, respectively, denoted by Γ-$E_{g,a}$, Γ-E_u, and Γ-$E_{g,b}$ in the order of increasing frequencies. Interestingly, only the Γ-$E_{g,a}$ phonons show an appreciable e-ph coupling corresponding to the transition of $1 \rightarrow 1'$.

IV. CONCLUSIONS

In summary, we have studied the phonon linewidths of the high-frequency optical-phonon modes in few-layer graphene. We found that there is a strong suppression of the e-ph interaction for these modes resulting from stacking patterns. The split optical-phonon modes in few-layer graphene are shown to only couple with the electronic bands of specific orbital symmetry and exhibit various e-ph interaction strengths. These features are well illustrated using a tight-binding model.

ACKNOWLEDGMENTS

We acknowledge helpful discussions with M. Wierzbowska and S. Piscanec. J.A.Y thanks F. Giustino and C.-H. Park for critical reading of the manuscript. This work is supported by the Department of Energy (Grant No. DE-FG02-97ER45632) and by the National Science Foundation (Grant No. DMR-08-20382). The computation used resources of the National Energy Research Scientific Computing Center (NERSC), which is supported by the U.S. Department of Energy (Grant No. DE-AC03-76SF00098), and the National Science Foundation Teragrid resources.

[1] C. Berger, Z. M. Song, T. B. Li, X. B. Li, A. Y. Ogbazghi, R. Feng, Z. T. Dai, A. N. Marchenkov, E. H. Conrad, P. N. First, and W. A. de Heer, J. Phys. Chem. B **108**, 19912 (2004).
[2] K. S. Novoselov, A. K. Geim, S. V. Morozov, D. Jiang, Y. Zhang, S. V. Dubonos, I. V. Grigorieva, and A. A. Firsov, Science **306**, 666 (2004).
[3] Y. Zhang, J. P. Small, W. V. Pontius, and P. Kim, Appl. Phys. Lett. **86**, 073104 (2005).
[4] Z. Yao, C. L. Kane, and C. Dekker, Phys. Rev. Lett. **84**, 2941 (2000).
[5] M. Lazzeri, S. Piscanec, F. Mauri, A. C. Ferrari, and J. Robertson, Phys. Rev. Lett. **95**, 236802 (2005).
[6] T. Kampfrath, L. Perfetti, F. Schapper, C. Frischkorn, and M. Wolf, Phys. Rev. Lett. **95**, 187403 (2005).
[7] N. Bonini, M. Lazzeri, N. Marzari, and F. Mauri, Phys. Rev. Lett. **99**, 176802 (2007).
[8] G. Grimvall, *The Electron-Phonon Interaction in Metals* (North-Holland, Amsterdam, 1981).
[9] A. Bostwick, T. Ohta, J. L. McChesney, T. Seyller, K. Horn, and E. Rotenberg, Solid State Commun. **143**, 63 (2007).
[10] J. González and E. Perfetto, Phys. Rev. Lett. **101**, 176802 (2008).
[11] M. Calandra and F. Mauri, Phys. Rev. B **76**, 205411 (2007).
[12] S. Y. Zhou, D. A. Siegel, A. V. Fedorov, and A. Lanzara, Phys. Rev. Lett. **101**, 086402 (2008).
[13] E. H. Hwang and S. Das Sarma, Phys. Rev. B **77**, 081412(R) (2008).
[14] A. C. Ferrari, Solid State Commun. **143**, 47 (2007).
[15] F. Giustino, Jonathan R. Yates, I. Souza, M. L. Cohen, and G. Louie, Phys. Rev. Lett. **98**, 047005 (2007).
[16] J. Menendez and M. Cardona, Phys. Rev. B **29**, 2051 (1984).
[17] J. Yan, Y. Zhang, P. Kim, and A. Pinczuk, Phys. Rev. Lett. **98**, 166802 (2007).
[18] M. Lazzeri, S. Piscanec, F. Mauri, A. C. Ferrari, and J. Robertson, Phys. Rev. B **73**, 155426 (2006).
[19] R. J. Nemanich, G. Lucovsky, and S. A. Solin, Solid State Commun. **23**, 117 (1977).
[20] T. Ohta, B. Bostwick, T. Seyller, K. Horn, and E. Rotenberg, Science **313**, 951 (2006).
[21] S. Latil and L. Henrard, Phys. Rev. Lett. **97**, 036803 (2006).
[22] T. Ohta, A. Bostwick, J. L. McChesney, T. Seyller, K. Horn, and E. Rotenberg, Phys. Rev. Lett. **98**, 206802 (2007).
[23] J. A. Yan, W. Y. Ruan, and M. Y. Chou, Phys. Rev. B **77**, 125401 (2008).
[24] We note that there are some further discussions of Kohn anomaly in monolayer and bilayer graphenes recently. See, e.g., W. K. Tse, Ben Yu-Kuang Hu, and S. Das Sarma, Phys. Rev. Lett. **101**, 066401 (2008) E. H. Hwang and S. Das Sarma, *ibid.* **101**, 156802 (2008).
[25] S. Baroni, S. de Gironcoli, and A. Dal Corso, Rev. Mod. Phys.

73, 515 (2001).
[26] S. Baroni, A. Dal Corso, S. de Gironcoli, and P. Giannozzi, http://www.pwscf.org.
[27] N. Troullier and J. L. Martins, Phys. Rev. B **43**, 1993 (1991).
[28] S. Piscanec, M. Lazzeri, F. Mauri, A. C. Ferrari, and J. Robertson, Phys. Rev. Lett. **93**, 185503 (2004).
[29] P. B. Allen, Phys. Rev. B **6**, 2577 (1972); P. B. Allen and R. Silberglitt, *ibid.* **9**, 4733 (1974).
[30] J. Yan, E. A. Henriksen, P. Kim, and A. Pinczuk, Phys. Rev. Lett. **101**, 136804 (2008).
[31] C.-H. Park, F. Giustino, M. L. Cohen, and S. G. Louie, Phys. Rev. Lett. **99**, 086804 (2007); Nano Lett. **8**, 4229 (2008).
[32] A. Rycerz, J. Tworzydło, and C. W. J. Beenakker, Nat. Phys. **3**, 172 (2007).
[33] A. R. Akhmerov and C. W. J. Beenakker, Phys. Rev. Lett. **98**, 157003 (2007).
[34] L. M. Woods and G. D. Mahan, Phys. Rev. B **61**, 10651 (2000).
[35] G. D. Mahan, Phys. Rev. B **68**, 125409 (2003).